

https://doi.org/10.1070/QEL17983

Generation of spherical laser-plasma clouds for modelling three-dimensional dynamic effects of artificial plasma injections in circumterrestrial space

Yu.P. Zakharov, V.A. Terekhin, I.F. Shaikhislamov, V.G. Posukh, P.A. Trushin, A.A. Chibranov, A.G. Berezutskii, M.S. Rumenskikh, M.A. Efimov

Abstract. **For the first time to solve the problems of laboratory modelling of cosmophysical phenomena of an explosive nature (active experiments of the AMPTE type, with barium injections into the magnetosphere), spherical laser plasma clouds (LPCs) were produced and applied (in experiments at the KI-1 test facility of the ILP SB RAS). Use was made of the classical four-beam scheme of irradiation (regular tetrahedron) of a polyethylene target ball (∅1 cm) by CO_2 laser radiation with an energy of up to 500 J. A high degree of symmetry of the expansion of a near-spherical LPC with a moderate velocity of ~100 km s^{-1} and an energy of up to 30 J has been achieved. The regimes of deceleration and formation of the spherical-LPC diamagnetic cavity were modelled for the first time, as well as the development of flute instability during the expansion of barium clouds across the geomagnetic field and the dynamics of these clouds along the field.**

Keywords: *CO_2 laser, four-beam scheme, ball target, spherical laser plasma cloud, magnetic field, laboratory simulation, active experiments in space, injection of barium plasma clouds, magnetosphere, flute-like and other plasma instabilities, Hall effects.*

1. Introduction

There are well-known examples of the application of the simplest scheme of symmetrical irradiation of spherical targets from four sides (in the geometry of a tetrahedron) at the initial stage of experiments on laser thermonuclear fusion in the USSR and abroad [1, 2], as well as in early model experiments [3, 4] in laboratory astrophysics at high-power laser facilities Helios and GekkoXII. However, in both cases, the sphericity of laser plasma clouds (LPCs) did not bring any advantages, and no essentially new results were obtained.

On the other hand, in many active experiments of recent decades on the injection of barium bunches into the ionosphere and magnetosphere of the Earth, primarily in the experiments of the AMPTE series [5], explosive methods are used to create close to spherical Ba vapour bunches, which are photoionised by the solar ultraviolet radiation in a characteristic time $t_i \approx 20$ s and then expand in the form of quasi-spherical plasma clouds with a front velocity $V_0 \approx 1$ km s^{-1}. Specifically, for example, in the best-known AMPTE experiment [5], as a result of the first injection in 1985 of a mass $M_0 \approx 1$ kg of barium (in the geomagnetic tail, with a magnetic field $B_0 \approx 8$ nT), the condition for the complete ionisation of Ba vapour up to the moment t_b of their deceleration by the field was obviously fulfilled. Indeed, in this case, for the radius R_b of deceleration by the magnetic field of a spherical plasma cloud (with energy $E_0 = 0.3M_0V_0^2$), according to Yu.P. Raiser's model [6], the following relationship can be written:

$$R_b = (3E_0/B_0^2)^{1/3} \approx 120 \text{ km}; \quad (1)$$

the corresponding deceleration time $t_b = R_b/V_0 \approx 120 \text{ s} \gg t_i$. This made it possible to study for the first time in the course of AMPTE [5] the dynamics of cloud–field interaction under the conditions of such a 'cosmic laboratory', including the structure and evolution of the diamagnetic cavity on the theoretical scale R_b (1), as well as the development of flute-like and other instabilities at the plasma-field boundary, which affect the size of the real cavity $R_c \leqslant R_b$. In particular, a lower-hybrid drift instability (LHDI [7]) was detected, which had previously been discovered in experiments with the LPCs [8, 9] in a vacuum magnetic field, during which the authors of Refs [10, 11] found for the first time the dependence of the real cavity size R_c (and its "lifetime" [12]) on the ion magnetisation criterion $\varepsilon_b = R_L/R_b$, where $R_L \propto (m/z)V_0$ is the 'directed' ion Larmor radius, and m and z are the ion mass and charge.

However, in view of the fact that such a dependence [13] can also be obtained (without involving the effects of LHDI turbulence) on the basis of a model that takes into account the Hall effect [14, 15] of dissipative-free field penetration into the plasma, we planned the 'Hall' experiment with spherical LPCs. The main advantage of this formulation of the model experiment is that it is precisely in the case of a spherical LPC that there is a two-dimensional analogue [16] of the formation of magnetic B_φ Hall fields in the presence of a background plasma in a uniform magnetic field.

This paper outlines the main data on the experimental setup and the first results of the generation of spherical LPCs on the KI-1 facility by irradiating a spherical target (∅1 cm, made of polyethylene) with LUI-2m CO_2 laser radiation [17] with an energy Q of up to 1 kJ and adjustable pulse shape. In this case, for comparable energies of the peak (up to 100 ns)

Yu.P. Zakharov, I.F. Shaikhislamov, V.G. Posukh, P.A. Trushin, A.A. Chibranov, A.G. Berezutskii, M.S. Rumenskikh, M.A. Efimov
Institute of Laser Physics, Siberian Branch, Russian Academy of Sciences, prosp. Akademika Lavrent'eva 15B, 630090 Novosibirsk, Russia; e-mail: ki1z@mail.ru;
V.A. Terekhin Russian Federal Nuclear Centre "All-Russian Research Institute of Experimental Physics", prosp. Mira, 37, 607188 Sarov, Nizhny Novgorod region, Russia

Received 19 October 2021
Kvantovaya Elektronika **52** (2) 155–159 (2022)
Translated by E.N. Ragozin

and microsecond tail (~200 J each), the target irradiation at an extremely low intensity [18] $q \sim 10^8$ W cm^{-2} (at $\lambda = 10.6$ μm) formed an LPC bunch with a front velocity $V_0 \approx 100$ km s^{-1}, an energy $E_0 \approx 25-30$ J, and a satisfactory degree of expansion symmetry.

Previously, in model experiments on KI-1 [18], use was made of quasi-spherical LPCs produced by double-sided irradiation of thin filaments or ball targets [9, 19] made of caprolon. The sufficiently symmetrical expansion of such LPCs was provided by the effects [18, 20] that equalise the temperatures near the target surface due to thermal conduction and absorption of the long-wavelength laser radiation (10.6 μm) in the corona. However, in experiments with such LPCs on the KI-1 facility (with a ball target and an additional source of up to 9-kG magnetic fields), there showed up the effect of jet formation [11] across such fields and along two laser beams. Therefore, in order to develop the laboratory simulative experiments [21] in a new parameter domain (primarily, at a high degree of ion magnetisation, with the criterion $\varepsilon_b \leqslant 0.3$), it became necessary to use more symmetrical target irradiation schemes, the simplest of which is the scheme based on a tetrahedron [22].

2. Setting up and results of experiments on the formation of spherical laser-plasma clouds in the four-sided irradiation of ball targets according to the scheme of an isosceles tetrahedron

Figure 1 shows the scheme for the formation and focusing of four CO_2 laser beams into the centre of the KI-1 vacuum chamber (5 m long and 1.2 m in diameter) onto a polyethylene ball target 10 mm in diameter to generate a spherically symmetric LPC. To maximise the spherical symmetry of the LPC in the framework of four-beam irradiation, we used the scheme of an isosceles tetrahedron, with the target at its centre and deflecting mirrors in each of its corners. Two radiation beams were injected into the vacuum chamber and were focused by two lenses with a focal length of 120 cm. Copper plates were placed after the lenses, reflecting about half the beam, while the second half passed further. At the final stage, copper mirrors at the vertices of the tetrahedron directed the beams to the target. This arrangement made it possible to minimise the path difference for the rays after the focusing lenses and achieve symmetrical coverage of all irradiation directions. Near the target, all radiation beams were focused into oval spots (with a highest intensity region of size ~10 × 12 mm). Several versions of target suspension were tested, the most suitable for our task was the mounting on a thin ceramic tube 2 mm in diameter, which inserted into the ball and oriented almost along the magnetic field. The longitudinal quasi-uniform and quasi-stationary magnetic field with strength B_0 up to 400 Gs was oriented along the chamber axis [like the incoming beams (*1*) in Fig. 1].

Figure 2 shows typical photographs of the LPC in a vacuum without a magnetic field, demonstrating a high degree of spherical symmetry of LPC expansion. Figure 3 shows the location of the main elements of probe diagnostics (probe inputs PE and IK) near the main section [or principal plane (PP)] of the KI-1 chamber, which passes through the target perpendicular to the z axis of the chamber. Due to the rotation of these inputs around their axes, the probes themselves on ceramic tubes can be moved apart both in the PP and at any angle to it (up to 90°, i.e., with their displacement along the z axis). Possible movements of the probes (and their 3D positions) were analysed using the Autocad program, and the probe positions were chosen from the conditions of not falling into the laser beams and the possibility of recording plasma flows from those target surface areas where the total radiation intensity of all four beams was likely to be minimal.

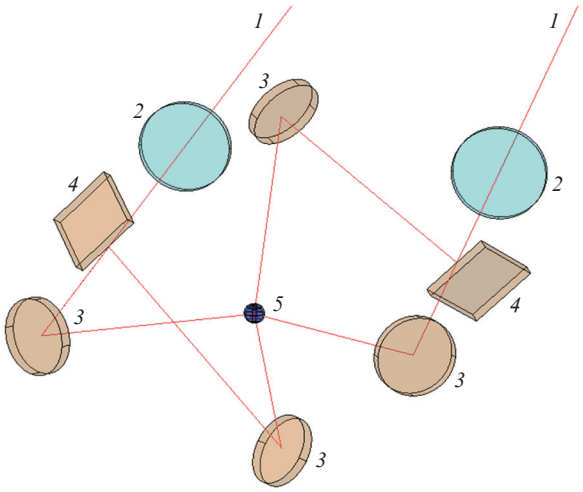

Figure 1. Schematic optical diagram of four-sided irradiation of ball targets (according to the isosceles tetrahedron scheme) on the KI-1 facility at the ILP SB RAS:
(*1*) incoming beams; (*2*) focusing lenses (NaCl) in the chamber with a total length of 5 m (diameter: 1.2 m); (*3*) copper mirrors; (*4*) copper beam splitters; (*5*) target (C_2H_4).

2.1. LPC diagnostics and parameters in the absence of a magnetic field

To monitor the degree of LPC expansion symmetry, three probe locations were chosen. The signals of double Langmuir probes were recorded using broadband circuits based on optocouplers [23]. Figure 4 shows the data on the initial symmetry in the form of dynamics (at different points) of the plasma density $n(t)$ of these probes (PE1, PE2), which is calculated from the general formula for the ion current collected by the probe on a thin cylindrical Langmuir probe in the plasma flow [24], $J_p = J_i \propto nVS_pF$, where $S_p = 2r_pl_p$; $r_p = 10$ μm $\leqslant \lambda_{De}$ is the probe radius; l_p is the probe length; F is a function of the probe potential; U_p is under 80 V; and λ_{De} is the Debye radius. Figure 5 shows similar data for collectors whose current $J_k = nVS_k$, where the geometric area S_k of the inlet opening is known and does not depend (in the saturation regime) on the collector voltage U_k. As a result (taking into account the secondary ion–electron emission coefficient γ), we calculated both the dynamics of the density $n(t)$ of the LPC in Fig. 4 and its total initial kinetic energy

$$E_0 = [2\pi R_p^4 \langle m/z \rangle/(1+\gamma)eF] \int (J_p/t^2)\,dt, \qquad (2)$$

where integration is performed from $t_0 = R_p/V_0$ to ∞; R_p is the distance from the probe to the target; and e is the electron charge.

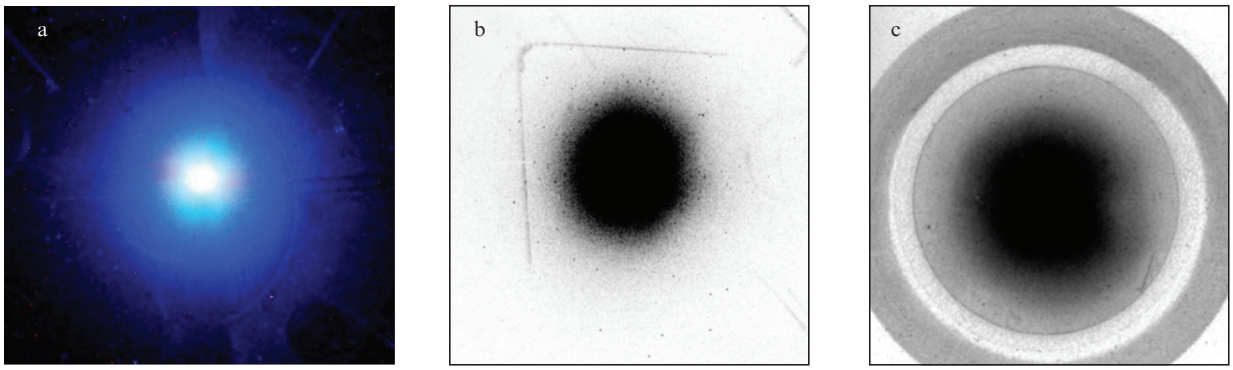

Figure 2. (Colour online) (a) Time-integrated photo of the LPC taken from the end of the chamber, as well as (b, c) photos made with an electro-optical converter from (b) the end and (c) side of the chamber, which were taken at the same point in time 1.5 μs (in different shots, with exposures $\Delta t = 0.5$ and 0.25 μs). The scales in Figs 2b and 2c are somewhat different. In Fig. 2b, at the top and bottom left, probe tubes are visible, the distance between the ends of which is 50 cm.

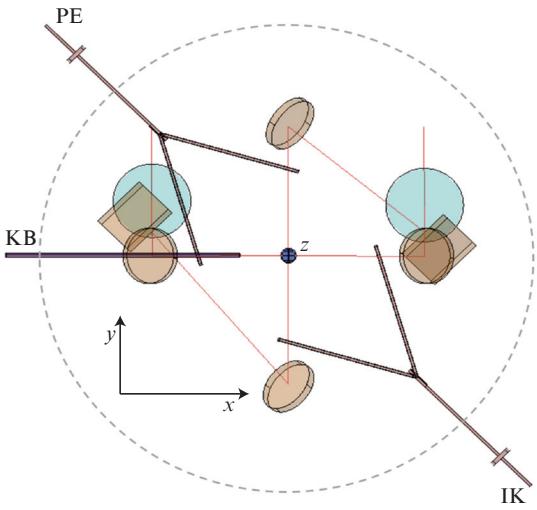

Figure 3. (Colour online) Location of the main elements of probe diagnostics, PE and IK inputs, in the area of the principal plane (PP) of the KI-1 camera in relation to the target (at the centre) and to the elements of the optical system (most of which are outside the PP). Each of the probes PE1, PE2 and IK1, IK2 represents two pairs of combinations (Langmuir probe + three-component magnetic probe) movable along the radius (by common rods: diagonal straight lines), and the mechanisms of the rods themselves can be rotated. At the ends of the rods inside the chamber there are holders of ceramic tubes, with probe pairs placed at their ends; the ends themselves can approach each other almost to the contact. KB is an ion collector, which moves along the radius $R(x)$ and measures the ion fluxes along z (at $z = \pm$ 68 cm, KB1 and KB2).

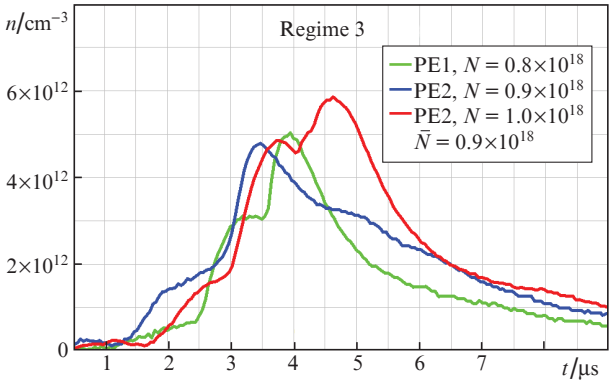

Figure 4. (Colour online) LPC density dynamics in the absence of a magnetic field at a distance $R = 25$ cm from the target (in various directions), including such shift from the Z axis (in the plasma generation regime n3); N is the total number of particles.

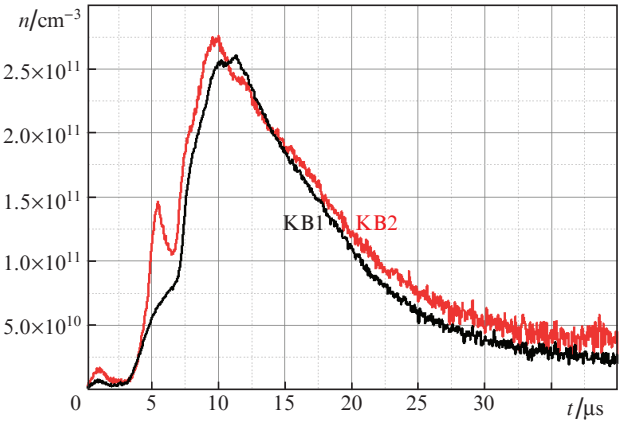

Figure 5. (Colour online) Density dynamics obtained for collectors KB1 and KB2 (in the regime of saturation of the ion current J_k to their flat receiving electrodes) in the absence of a magnetic field, at distances along the z axis = ± 68 cm from the target (near the chamber axis, at $R \le 1$ cm).

Figure 5 shows the collector data on the LPC density dynamics in the direction along the field [similar data on the LPC energy in this direction were obtained from expression (2) for $F = 1$]. The initial data of probes PE1, PE2 on the density in Fig. 4 [the arrival time and magnitude of signals at 25 cm in regime 3 (plasma production regime)] are in good agreement with the data of collectors in other directions in Fig. 5 (at distances $z = \pm 68$ cm). As a result, the preliminary average data (and single-shot data) on the initial energy E_0 and on the total number of particles N are quite close: for probes PE1, PE2 and IK1, IK2 – 23 J for 0.9×10^{18}; and for collectors, 21 and 27 J for 1.25×10^{18}. Note that before the main experiments, all of these probe diagnostics were mutually calibrated under conditions of a hydrogen background plasma from a theta-pinch type source with a density $n_* \sim 10^{13}$ cm^{-3} (at their close location).

2.2. LPC parameters based on the characteristics of a diamagnetic cavity and plasma dynamics in a uniform magnetic field

The main measurements were carried out in a sufficiently strong magnetic field $B_0 = 400$ Gs to ensure the conditions for the magnetisation of LPC ions according to the criterion $\varepsilon_b = R_L/R_b < 1$ and the formation of a cavity with a radius $R_c \approx R_b$. Indeed, at the determined average LPC energy $E_0 \approx 23.5$ J, the spatial scale of cloud deceleration (1) across the field should be $R_b \approx 16.4$ cm for the ion Larmor radius $R_L \approx 7.5$ cm (for the carbon ion charge $Z = 3$ [25] and the LPC front velocity $V_0 \approx 100$ km s^{-1}), so that the criterion for effective plasma–field interaction is realised and $\varepsilon_b \approx 0.46$ (<1) even without the inclusion of protons in the LPC. Then, according to the generalised experimental data [10], one could expect the actual cavity size $R_c \approx 15.6$ cm, while in our experiments [29.04.2021 and 25.05.2021 (Fig. 6)] an experimental cavity with a radius of only $R_{ce} \approx 14$ and 15 cm, which is quite close to what is expected at such an LPC energy and a given average $E_0 \approx 23.5$ J. In all cases of a strong field, a significant plasma deceleration was observed (Figs 7, 8), and the discrepancy between the cavity sizes R_c and R_{ce} can be associated with the changes in the shape and transverse dimensions of the LPC due to its almost free expansion along the field [26],

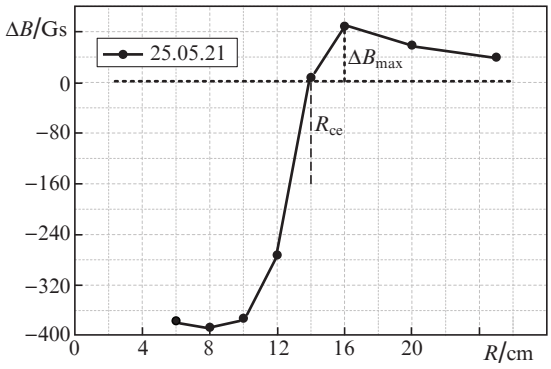

Figure 6. Structure of the diamagnetic cavity of a spherical LPC in a maximum magnetic field $B_0 = 400$ G. The point in time is 4.2 μs, for the maximum cavity size $R_{ce} \approx 14$ cm.

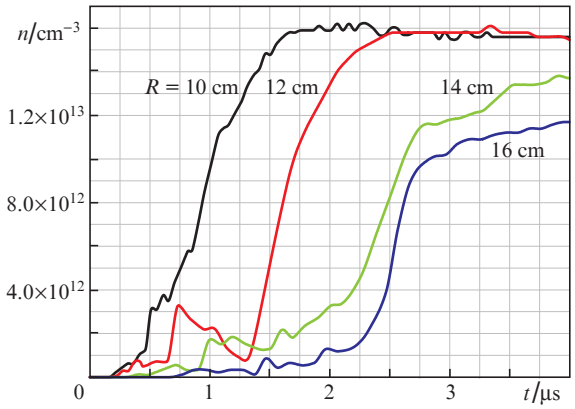

Figure 7. (Colour online) Oscillogram (25.05.2021, probe PE1) showing the deceleration of the LPC front at various distances R across a strong magnetic field of 400 G, according to the ion flux density in arbitrary density units.

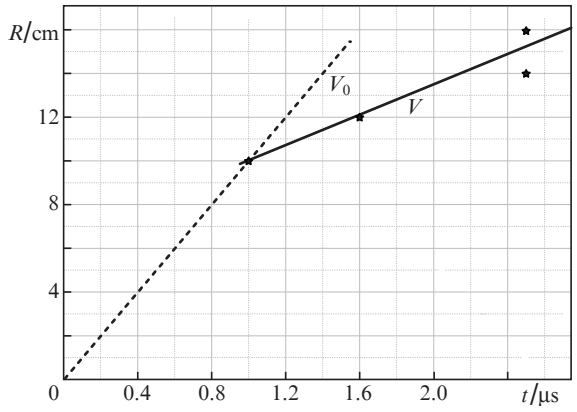

Figure 8. $R-t$ diagram of the LPC front deceleration in a strong magnetic field $B_0 = 400$ Gs (constructed from the data of Fig. 7). The transition from the initial velocity $V_0 \approx 100$ km s^{-1} to a significantly reduced one (down to ~30 km s^{-1}) occurs on a scale of ~14 cm (± 2 cm), close to the calculated stagnation radius $R_b \approx 16$ cm [6].

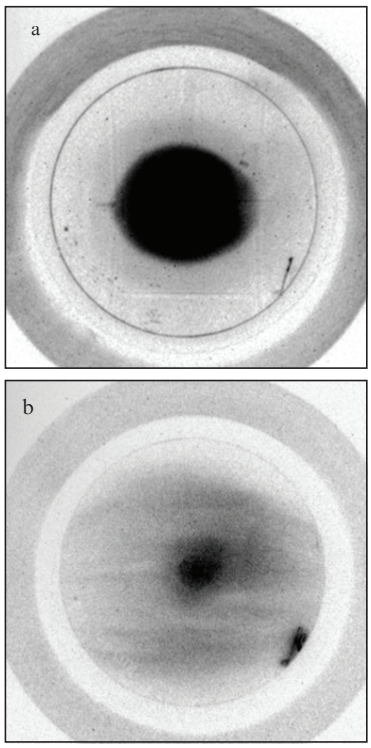

Figure 9. Photographs of the LPC taken in the central section 'from the side' of the vacuum chamber at (a) $t = 1.5$ μs, $\Delta\tau = 0.5$ μs and (b) $t = 3.65$ μs, $\Delta\tau = 1$ μs; magnetic field $B_0 = 400$ Gs (28.05.2021). Figure 9b shows the development of flutes along the field.

which is noticeable in the images of a high-speed photorecorder (Fig. 9) at these stages.

Late in the interaction of LPC bunches with the field ($t \approx 3-4$ μs $\approx 2R_b/V_0$), also possible is the influence of the rapid development of anomalous flute-like instability (Fig. 10) at finite $\varepsilon_b \sim 1$ [27, 28] (the effect of anomalous flute instability on the cavity dimensions was studied in detail in Ref. [11]). In the case of expansion of such an LPC in a weak field $B_0 = 70-100$ Gs at $\varepsilon_b \approx 1.1$ ($\geqslant 1$), the LPC front does not slow down at all (Fig. 11), at least on the studied scales up to 33 cm (with the calculated $R_b \approx 50$ cm).

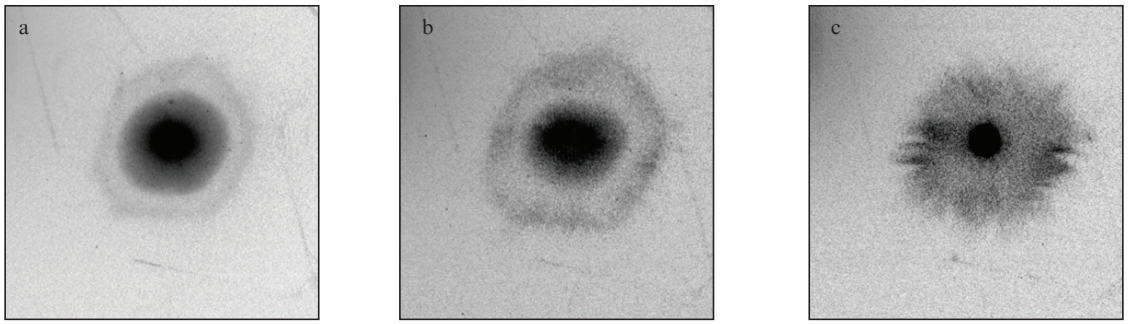

Figure 10. LPC photographs for (a) $t = 2$ μs, $\Delta\tau = 0.5$ μs, (b) $t = 2.5$ μs, $\Delta\tau = 0.5$ μs, and (c) $t = 3.5$ μs, $\Delta\tau = 1$ μs; the magnetic field, $B_0 = 400$ Gs. Approximately 20 to 24 flutes can be observed.

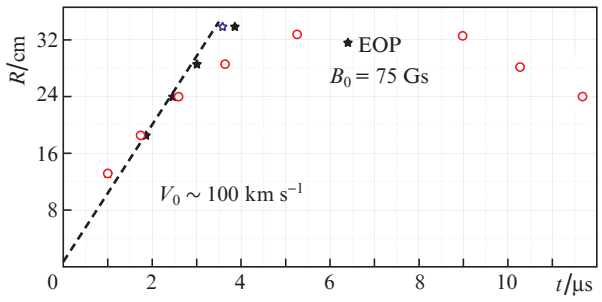

Figure 11. (Colour online) $R-t$ diagram of the propagation of the LPC front in the regime of weakly magnetised ions without significant deceleration of the cloud for $\varepsilon_b = R_L/R_b \approx 1.1 \geqslant 1$ (in a field of 70 Gs): LPC density front (★), radii of the edges of the cavity under strong displacement (○), LPC density front in the absence of magnetic field (☆). The EOP point corresponds to the moment when the electrooptical converter records the arrival of the LPC (in the form of flutes) at the metal mounting ring ∅90 cm (inside the KI-1 chamber, near the PP). The electrooptical converter is triggered at the point in time $t \approx 6.5$ μs with the maximum exposure $\Delta\tau = 5$ μs.

3. Conclusions

The simplest scheme of symmetrical CO_2 laser irradiation of a spherical target in the four-beam geometry of a regular tetrahedron was successfully implemented. As a result, the interaction of a close to spherically symmetric LPC with a magnetic field was realised for the first time for the purposes of laboratory modelling of cosmophysical phenomena of explosive nature (active experiments of the AMPTE type in the magnetosphere). We recorded the effects of diamagnetic cavity formation and the deceleration of the LPC across the field (and expansion along it) with the development of an anomalous flute-like instability (of the Rayleigh–Taylor type) at the front of the LPC. The achieved characteristics of the spherical LPC provide unique opportunities for studying the 3D effects of anomalously fast cavity collapse due to possible Hall non-dissipative processes of magnetic field penetration.

Acknowledgements. This work was partly supported by the Russian Foundation for Basic Research (Grant No. 18-29-21018).

References

1. Zaretskii A.I., Kirillov G.A., Kormer S.B. *Sov. J. Quantum Electron.*, **13**, 468 (1983) [*Kvantovaya Elektron.*, **10**, 756 (1983)].
2. Kitagawa Y., Miyanaga N., Hama H., et al. *Phys. Rev. Lett.*, **51**, 570 (1983).
3. Borovsky J.E., Morris B., et al. *Astrophys. J.*, **280**, 802 (1984).
4. Kuramitzu Y., Matsukiyo S., et al. *J. Phys.: Conf. Ser.*, **688**, 012056 (2016).
5. Bernhardt P.A., Roussel-Dupre R.A., et al. *J. Geophys. Res.*, **92A**, 5777 (1987).
6. Raizer Yu.P. *Prikl. Matem. Tekh. Fiz.*, (6), 19 (1963).
7. Gladd N.T., Brecht S.H. *Phys. Fluids*, **B3**, 3232 (1991).
8. Okada S., Sato K., Sekiguchi T. *Jpn. J. Appl. Phys.*, **20**, 157 (1981).
9. Antonov V.M., Zakharov Yu.P., Orishich A., et al, in *Trudy VI Vsesoyuznoi Konf. Fizika Nizkotemperaturnoi Plazmy* (Proc. VI All-Union. Conf. Physics of Low-Temperature Plasma) (Leningrad, 1983) Vol. II, pp 198–200.
10. Zakharov Yu.P., et al. *Fiz. Plazmy*, **12**, 1170 (1986).
11. Zakharov Yu.P., et al. *Fiz. Plazmy*, **32**, 207 (2006).
12. Zakharov Yu.P., Melekhov A.V., Ponomarenko A.G., et al. *Jpn. J. Plasma Fusion Res.*, **2**, 348 (1999).
13. Zakharov Yu.P., Orishich A.M., Ponomarenko A.G., Shaikhislamov I.F., in *Proc. 10th European School Plasma Physics* (Tbilisi, 1990) pp 184–202.
14. Vainshtein S.I. et al. *Phys. Rev. E*, **61**, 4422 (2000).
15. Bergel'son A.M., Raizer Yu.P., Surzhikov S.T. *Prikl. Mat. Tekh. Fiz.*, (3), 22 (1991).
16. Bashurin V.P., Golubev A.I., Terekhin V.A. *Prikl. Mat. Tekh. Fiz.*, (6), 10 (1983).
17. Orishich A.M., Posukh V.G., Snytnikov V.N., in *Moshchnye CO_2-lazery dlya plazmennykh eksperimentov i tekhnologii* (High-Power CO_2 Lasers for Plasma Experiments and Technology) (Novosibirsk: ITPM, 1986) pp 56–76.
18. Zakharov Yu.P., Orishich A.M., Ponomarenko A.G. *Lazernaya plazma i laboratornoe modelirovanie nestatsionarnykh kosmicheskikh protsessov* (Laser-Produced Plasma and Laboratory Modelling of Nonstationary Cosmic Processes) (Novosibirsk: ITPM, 1988).
19. Avdyeva A.A., Zakharov Yu.P., Maksimov V.V. et al. *Prikl. Mat. Tekh. Fiz.*, (6), 62 (1989).
20. Gus'kov S.Yu., Zverev V.V., Karpov V.Ya., et al., in *Trudy FIAN* (Proc. of P.N. Lebedev Phys. Inst. Akad. Nauk SSSR) (Moscow: Nauka, 1986) Vol. 170, p. 93.
21. Zakharov Yu.P., Terekhin V.A., Shaikhislamov I.F., et al., in *Techn. Dig. MPLP-2021. IX Int. Symp.* (Novosibirsk, 2021) pp 170–172.
22. Howard J.E. *Appl. Opt.*, **16**, 2764 (1977).
23. Zakharov Yu.P., In *Moshchnye CO_2-lazery dlya plazmennykh eksperimentov i tekhnologii* (High-Power CO_2 Lasers for Plasma Experiments and Technology) (Novosibirsk: ITPM, 1986) p. 125.
24. Zakharov Yu.P., et al. *Quantum Electron.*, **46**, 399 (2016) [*Kvantovaya Elektron.*, **46**, 399 (2016)].
25. Garban C., et al. *J. Physique Lett.*, **39**, L165 (1978).
26. Metelkin E.V., Sorokin V.M. *Geomagnetizm i Aeronomiya*, **28**, 756 (1988).
27. Zakharov Yu.P., Orishich A.M., Ponomarenko A.G., et al., in *ESA Proc. Joint Varenna-Abastumani Int. School Workshop Plasma Astrophys* (Sukhumi, USSR, 19–28 May 1986) p. 37.
28. Ripin B.H., McLean E.A., Manka C.K., et al. *Phys. Rev. Lett.*, **59**, 2299 (1987).